

CHAPTER 1

FUNDAMENTAL MODELS AND MEASUREMENTS FOR ULTRASONIC NONDESTRUCTIVE EVALUATION SYSTEMS

Lester W. Schmerr Jr.

*Center for Nondestructive Evaluation and the Dept. of Aerospace Engineering
Iowa State University Ames, Iowa 50011
lschmerr@cnde.iastate.edu*

It will be shown that it is possible to completely characterize an ultrasonic nondestructive flaw measurement system and simulate the measured flaw signals. This characterization includes the pulser/receiver, cabling, and transducers present as well as the propagating and scattered acoustic/elastic wave fields. All the elements of this comprehensive ultrasonic measurement model will be discussed as well as practical methods for obtaining those elements through a combination of models and measurements.

1. Introduction

Ultrasound is widely used for both medical evaluations and industrial inspections. In medical applications the ultrasound is typically propagating in tissue and the interactions of the sound with objects such as tumors are normally displayed in the form of ultrasonic images for evaluation by a physician. In industrial nondestructive evaluation (NDE) ultrasonic tests the ultrasonic waves are traveling in structural materials or components and the focus is often on evaluating those components for flaws such as cracks. While the results of the interaction of the sound with flaws can also be displayed as an ultrasonic image, a more common type of display used in industrial inspections is a received voltage versus time trace, $\tilde{V}_R(t)$, on an oscilloscope, called an *A-scan*, as shown in Fig. 1 for a typical immersion ultrasonic NDE flaw inspection system. Since images are generated by processing combinations of such A-scans, A-scan data provides the fundamental basis for describing the output of both medical and industrial ultrasonic systems.

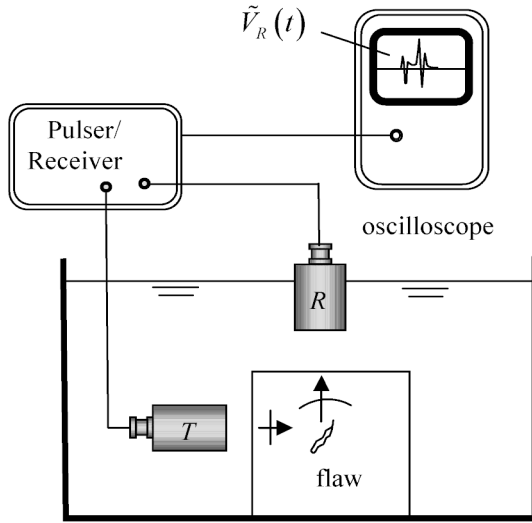


Figure 1. An ultrasonic pitch-catch flaw measurement system.

The basic components of the ultrasonic inspection system of Fig. 1 are the pulser/receiver, the cabling, the transducers, and the acoustic/elastic wave propagation and scattering processes present. The pulser section of the pulser/receiver generates short electrical pulses which travel through the cabling to the transmitting transducer. The transducer converts these electrical pulses into acoustic pulses at its acoustic output port. In the immersion setup of Fig. 1 these acoustic pulses first travel as a beam of sound in the fluid. This sound beam is transmitted into the solid component being inspected and the beam interacts with any flaws that are present. The flaw generates scattered wave pulses traveling in many directions, but some of these pulses reach the receiving transducer which then converts them into electrical pulses. These electrical pulses travel again through cabling to the receiver section of the pulser/receiver, where they are amplified and displayed as a received A-scan voltage, $\tilde{V}_R(t)$, as a function of the time t .

If we assume the components of the ultrasonic system shown in Fig. 1 can be represented as *linear time-shift invariant (LTI) systems* [1], then the output voltage pulse, $\tilde{V}_R(t)$, can be written as a convolution integral of the form

$$\tilde{V}_R(t) = \int_{-\infty}^{+\infty} \tilde{s}(\tau) \tilde{f}_A(t-\tau) d\tau, \quad (1.1)$$

where $\tilde{s}(t)$ is a function that characterizes all the electrical and electrical-to-acoustic and acoustic- to-electrical elements present (the pulser/receiver, cabling,

and transducers) and $\tilde{t}_A(t)$ is a function that contains the acoustic/elastic wave propagation and scattering processes occurring in the fluids and solids. We will find it convenient not to deal directly with these time dependent functions. Instead, we will model the ultrasonic system of Fig. 1 in the frequency domain by applying the Fourier transform to whatever pulses are present. In this chapter the Fourier transform and its inverse are defined as [2]:

$$g(f) = \int_{-\infty}^{+\infty} \tilde{g}(t) \exp(2\pi i f t) dt$$

$$\tilde{g}(t) = \int_{-\infty}^{+\infty} g(f) \exp(-2\pi i f t) df$$
(1.2)

for a time-domain function, $\tilde{g}(t)$, and its frequency domain spectrum, $g(f)$, where t is time (usually measured in μsec) and f is frequency (usually measured in megaHertz (MHZ)). In Eq. (1.2) $i = \sqrt{-1}$. For an LTI system, Eq. (1.1) becomes in the frequency domain simply a product relationship, *i.e.* [1]:

$$V_R(f) = s(f)t_A(f),$$
(1.3)

where $V_R(f)$ are the frequency components(spectrum) of $V_R(t)$, $s(f)$ is the *system function*, and $t_A(f)$ is the *acoustic/elastic transfer function*.

Even though Eq. (1.3) is very simple in form, it also is extremely useful. We will show that it is possible to measure the system function directly in a reference calibration experiment and to model the contributions of the complex propagating and scattered waves present in the acoustic/elastic transfer function. This means that through a combination of models and measurements it is possible to synthesize the frequency components of the measured signals for many ultrasonic NDE setups. An inverse Fourier transform (done with a Fast Fourier Transform (FFT)) then yields a prediction of the measured A-scan signals. To make this approach quantitative we need to explicitly define the acoustic/elastic transfer function and the system function. The physical meaning of both of these functions will be described in detail in the following sections.

2. The Acoustic-Elastic Transfer Function

Dang *et al.* [3, 4] have used mechanical reciprocity principles to develop an expression for the acoustic/elastic transfer function, $t_A(f)$, for the immersion setup of Fig. 1. They found

$$t_A(f) = \frac{1}{Z_r^{T:a} v_T^{(1)} v_R^{(2)}} \int_{S_f} (\boldsymbol{\tau}^{(1)} \cdot \mathbf{v}^{(2)} - \boldsymbol{\tau}^{(2)} \cdot \mathbf{v}^{(1)}) dS. \quad (1.4)$$

In Eq. (1.4) two solutions are present. The first solution (labeled as state (1)) is when the transmitting transducer T is radiating into the fluid with an average velocity, $v_T^{(1)}(f)$, on its face. In this solution the waves arriving at the flaw from the transducer and those scattered from the flaw generate the stress vector, $\boldsymbol{\tau}^{(1)}$, and velocity, $\mathbf{v}^{(1)}$, on the surface of the flaw, S_f . The second solution (labeled as state (2)) is for the case when the receiving transducer R is acting as a transmitter with an average velocity, $v_R^{(2)}(f)$, on its face and the flaw is absent, so that $\boldsymbol{\tau}^{(2)}, \mathbf{v}^{(2)}$ are the stress vector and velocity, respectively, on S_f due the arriving waves only. The quantity $Z_r^{T:a}$ is the *acoustic radiation impedance* of the transmitting transducer, T . If we model the transmitting transducer as a piston probe where the output velocity is spatially uniform over the acoustic output port of the transducer, then at the high frequencies normally found in NDE tests it can be shown that $Z_r^{T:a} = \rho_1 c_{p1} S_T$, where ρ_1, c_{p1} are the density and wave speed of the fluid the transducer is radiating into and S_T is the area of the active face of the transducer [3]. Commercial ultrasonic NDE transducers can often be very successfully modeled as piston probes so that in this case the acoustic radiation impedance is a simple, known quantity. Equation (1.4) relies primarily on assumptions of linearity and reciprocity of the ultrasonic measurement system so that although it was explicitly developed for the immersion setup of Fig.1 it is also applicable to most ultrasonic bulk wave measurement systems, including contact cases and those using angle beam shear waves. Since the stress vector and velocity fields on the surface of the flaw for states (1) and (2) in Eq. (1.4) are divided by the average velocities acting on the faces of the transmitting transducers in those two states, we only need to know “normalized” stress vector and velocity fields at the flaw for states (1) and (2), *i.e.* when the transmitting transducers have unit average velocity on their faces. These normalized stress vectors and velocity vectors in states (1) and (2) on the surface of the flaw can, therefore, be obtained directly from models if one has a sufficiently general transducer beam model and flaw scattering model for the ultrasonic flaw measurement setup under consideration and one does not need to know the actual velocities generated on the transducer faces to obtain this transfer function.

If we place Eq. (1.4) into Eq. (1.3) and assume that the system function is known or can be measured then we have a general *ultrasonic measurement model* given by:

$$V_R(f) = \frac{s(f)}{Z_r^{T:a} v_T^{(1)} v_R^{(2)}} \int_{S_f} (\boldsymbol{\tau}^{(1)} \cdot \mathbf{v}^{(2)} - \boldsymbol{\tau}^{(2)} \cdot \mathbf{v}^{(1)}) dS. \tag{1.5}$$

A form similar to Eq. (1.5) was first derived by Bert Auld in 1979 [5] and has been used world-wide by many researchers in conjunction with analytical or numerical wave propagation and scattering models that can evaluate the $(\boldsymbol{\tau}, \mathbf{v})$ fields for states (1) and (2). Many of these applications of Eq. (1.5) can be found in past volumes of the Review of Progress in Quantitative Nondestructive Evaluation [6].

Now, assume that the incident waves in both these states in the vicinity of the flaw can be written in quasi-plane wave form, *i.e.*

$$\begin{aligned} \mathbf{v}^{(1);inc} &= v_T^{(1)}(f) \hat{V}^{(1)}(\mathbf{x}, f) \mathbf{d}^{(1)} \exp\left[ik_{\beta 2} \mathbf{e}^{(1)} \cdot \mathbf{x} \right] \\ \mathbf{v}^{(2)} &= v_R^{(2)}(f) \hat{V}^{(2)}(\mathbf{x}, f) \mathbf{d}^{(2)} \exp\left[ik_{\alpha 2} \mathbf{e}^{(2)} \cdot \mathbf{x} \right], \end{aligned} \tag{1.6}$$

where $\hat{V}^{(m)}$ ($m = 1, 2$) are complex-valued “amplitudes” that represent the incident velocity fields normalized by the driving velocities $v_T^{(m)}$ ($m = 1, 2$) and $\mathbf{d}^{(m)}$ are the polarization vectors for these incident velocity fields in both states ($m = 1, 2$). The parameters $k_{\alpha 2} = 2\pi f / c_{\alpha 2}$ and $k_{\beta 2} = 2\pi f / c_{\beta 2}$ are the wave numbers in the solid surrounding the flaw for the incident waves in states (1) and (2), respectively, where α and β denote the incident bulk wave type (p or s) present and $(c_{\alpha 2}, c_{\beta 2})$ are their wave speeds. Note that in state (2) the incident velocity field is the entire field present since the flaw is absent while in state (1) this field is only part of the total field, so that this difference has been indicated explicitly in Eq. (1.6) by labeling the incident field in state (1) with the superscript “*inc*”. If we place the expressions of Eq. (1.6) into Eq. (1.5) and also assume the amplitude terms in Eq. (1.6) do not vary significantly over the surface of the flaw, then Eq. (1.5) reduces to [1]:

$$V_R(f) = s(f) \hat{V}_0^{(1)}(f) \hat{V}_0^{(2)}(f) A(f) \left[\frac{4\pi\rho_2 c_{\alpha 2}}{-ik_{\alpha 2} Z_r^{T:a}} \right], \tag{1.7}$$

where $\hat{V}_0^{(m)}(f) \equiv \hat{V}^{(m)}(\mathbf{x}_0, f)$ ($m = 1, 2$) are the beam “amplitudes” evaluated at some fixed point, \mathbf{x}_0 , in the vicinity of the flaw (usually taken as at the flaw “center”), ρ_2 is the density of the solid medium surrounding the flaw, and $A(f)$ is a scalar component of the vector plane wave far-field scattering amplitude of the flaw, a term we will discuss in more detail in section 1.4. A form similar to Eq. (1.7) was first derived by Thompson and Gray in 1983 [7] and is referred to as the *Thompson-Gray measurement model*. Although Eq. (1.7)

is less general than Eq. (1.5), it explicitly identifies all the contributions to the measured voltage response in a modular form which makes it an extremely useful tool for analyzing ultrasonic NDE flaw inspection systems. The flaw response, for example, is contained entirely in $A(f)$. The effects of the instrumentation and transducers are contained in the system function, $s(f)$, and the ultrasonic beams incident on the flaw are given by the terms $\hat{V}_0^{(m)}(f)$. The remaining term in Eq. (1.7) is just a combination of simple, known parameters. This modularity of Eq. (1.7) has been exploited in numerous quantitative flaw studies, many of which can also be found in past volumes of the Review of Progress in Quantitative Nondestructive Evaluation [6].

In both Eq. (1.5) and Eq. (1.7) the acoustic/elastic transfer function is defined implicitly in terms of the fields present in a flaw measurement. It is also possible to obtain more explicit analytical expressions for the acoustic/elastic transfer function in some simple calibration setups. Such setups are used for determining the system function, $s(f)$, as well as finding transducer and other system parameters. Figure 2 shows two examples of setups where the acoustic/elastic transfer function is known. In Fig. 2(a), a circular, planar piston P-wave transducer of radius a generates and receives the waves reflected from a flat fluid-solid interface. For this pulse-echo immersion setup the acoustic/elastic transfer function, $t_A^{planar}(f)$ is [1]

$$t_A^{planar}(f) = R_{12} \exp(2ik_{p1}D) \exp[-2\alpha_{p1}(f)D] \tilde{D}_p(k_{p1}a^2/2D) \quad (1.8)$$

with

$$\tilde{D}_p(u) = 2[1 - \exp(iu)\{J_0(u) - iJ_1(u)\}]. \quad (1.9)$$

Here R_{12} is the plane wave reflection coefficient for the interface, based on the ratio of the reflected pressure to that of the incident pressure given by

$$R_{12} = \frac{\rho_2 c_{p2} - \rho_1 c_{p1}}{\rho_2 c_{p2} + \rho_1 c_{p1}}, \quad (1.10)$$

where ρ_1, c_{p1} and ρ_2, c_{p2} and are the density and compressional wave speed of the fluid and solid, respectively, $k_{p1} = 2\pi f / c_{p1}$ is the wave number for waves traveling in the fluid, a is the radius of the transducer, and D is the distance from the transducer to the fluid-solid interface. The functions $J_0(u), J_1(u)$ are Bessel functions of the first kind of order zero and one, respectively, and $\alpha_{p1}(f)$ is the frequency dependent attenuation of P-waves traveling in the fluid. For degassed

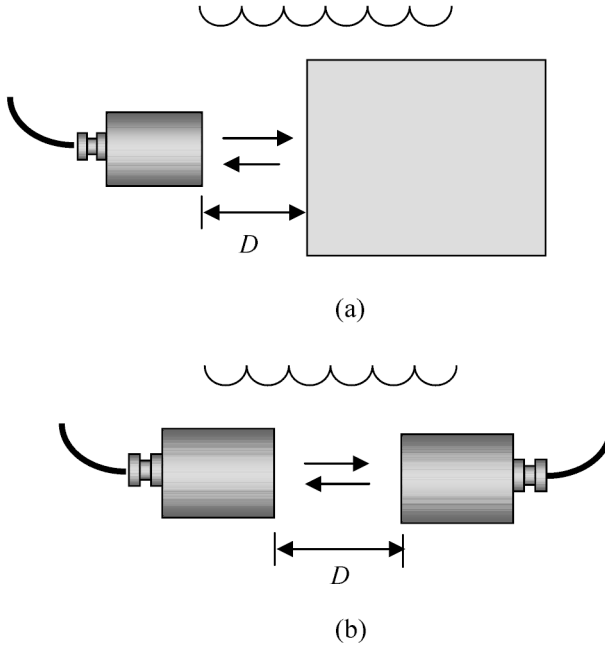


Figure 2. (a) A pulse-echo reference ultrasonic setup and (b) a pitch-catch ultrasonic reference setup.

water, this attenuation function has been experimentally determined [1]. In Eq. (1.8) the first three terms on the right hand side of that equation represent a plane wave that has been reflected from the interface and has returned to the transducer. Thus the \tilde{D}_p function is a *diffraction correction* that accounts for the fact that the transducer generates a reflected beam of sound, not just a plane wave. Although Eq. (1.8) is for a planar transducer, it can also be modified to determine the acoustic/elastic transfer function, $t_A^{sph}(f)$, for a circular, spherically focused piston transducer with a geometrical focal length, R_0 , in the setup of Fig. 2(a) where the distance $D = R_0$. In that case, one finds [8]

$$t_A^{sph}(f) = R_{12} \exp(2ik_{p1}R_0) \exp[-2\alpha_{p1}(f)R_0] [\tilde{D}_p(k_{p1}a^2/2R_0)]^*, \quad (1.11)$$

where $[]^*$ denotes the complex-conjugate. In a similar fashion, for a rectangular piston transducer in the pulse-echo immersion setup of Fig. 2(a) the acoustic/elastic transfer function, $t_A^{rect}(f)$, is [9]:

$$t_A^{rect}(f) = R_{12} \exp(2ik_{p1}D) \exp[-2\alpha_{p1}(f)D] \tilde{D}_p^{rect}(k_{p1}a^2/2D) \quad (1.12)$$

with

$$\tilde{D}_p^{rect} = \frac{4}{i} \left\{ F\left(\sqrt{2k_{p1}a^2/\pi D}\right) + \frac{i}{\pi\sqrt{2k_{p1}a^2/\pi D}} \left[\exp(ik_{p1}a^2/D) - 1 \right] \right\} \cdot \left\{ F\left(\sqrt{2k_{p1}b^2/\pi D}\right) + \frac{i}{\pi\sqrt{2k_{p1}b^2/\pi D}} \left[\exp(ik_{p1}b^2/D) - 1 \right] \right\}, \tag{1.13}$$

where $F(x)$ is the Fresnel integral

$$F(x) = \int_0^x \exp(i\pi t^2/2) dt \tag{1.14}$$

and the lengths of the two sides of the transducer are $(2a, 2b)$, respectively. Similarly, for a cylindrically focused rectangular piston transducer with geometrical focal length, R , along the side of the transducer whose length is $2b$, and where the distance $D = R$ we can also easily modify Eq. (1.12) to obtain the acoustic/elastic transfer function, $t_A^{cyl}(f)$, for this cylindrically focused transducer as [9]

$$t_A^{cyl}(f) = R_{12} \exp(2ik_{p1}R) \exp[-2\alpha_{p1}(f)R] \cdot \frac{4}{i} \left\{ F\left(\sqrt{2k_{p1}a^2/\pi R}\right) + \frac{i}{\pi\sqrt{2k_{p1}a^2/\pi R}} \left[\exp(ik_{p1}a^2/R) - 1 \right] \right\} \cdot \left\{ F\left(\sqrt{2k_{p1}b^2/\pi R}\right) + \frac{i}{\pi\sqrt{2k_{p1}b^2/\pi R}} \left[\exp(ik_{p1}b^2/R) - 1 \right] \right\}^* \tag{1.15}$$

All of the examples so far have been for pulse-echo immersion setups. For the pitch-catch setup of Fig. 2(b), the acoustic/elastic transfer function for a pair of circular, planar piston transducers, both having the same radius, a , is given simply by [1]

$$t_A(f) = \exp(ik_{p1}D) \exp[-\alpha_{p1}(f)D] \tilde{D}_p(k_{p1}a^2/D), \tag{1.16}$$

involving the same diffraction correction function, \tilde{D}_p , as before.

We have given these examples to show a few important cases where the acoustic/elastic transfer function can be obtained but there are many other calibration setups where this transfer function is also known [10]. For more complex calibration configurations (such as found in contact and angle beam transducer setups) where analytical expressions for this transfer function cannot

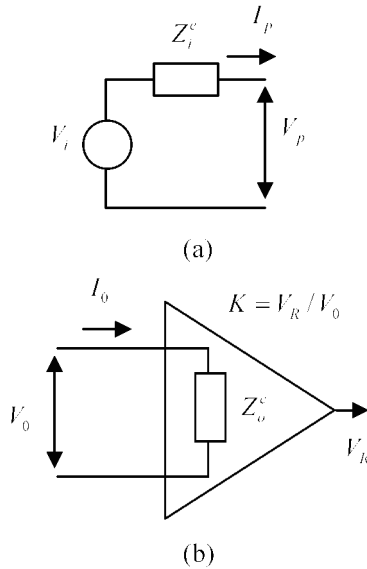


Figure 3. (a) A model of the pulser section of a pulser/receiver as a voltage source and an electrical impedance, and (b) a model of the receiver section as an electrical impedance and a gain factor.

be obtained, it is possible to numerically determine the acoustic/elastic transfer function by use of a transducer beam model [11].

3. The System Function

It is necessary to model the acoustic/elastic transfer function in some form since it involves the propagation and scattering of wave fields in fluids and solids, fields that are often not able to be measured directly. The system function, however, can be measured in reference setups (such as those just discussed) where the acoustic/elastic transfer function is known. For any such reference setup, if the acoustic elastic transfer function is $t_A^{ref}(f)$ and the frequency spectrum, $V_R^{ref}(f)$, of the received signal is measured, then by Eq. (1.3) we have

$$s(f) = \frac{V_R^{ref}(f)}{t_A^{ref}(f)}, \tag{1.17}$$

i.e. we can obtain the system function by deconvolution. In practice the division in Eq. (1.17) is carried out with the aid of a *Wiener filter* to desensitize the deconvolution process to noise. The equivalent Wiener filter form is [12]

$$s(f) = \frac{V_R^{ref}(f) [t_A^{ref}(f)]^*}{|t_A^{ref}(f)|^2 + \varepsilon^2 \max\{|t_A^{ref}(f)|^2\}}, \quad (1.18)$$

where ε is a constant that is chosen to characterize the noise level present in the measurement. As $\varepsilon \rightarrow 0$ Eq. (1.18) reduces to Eq. (1.17).

The system function characterizes all the electrical and electromagnetic components of the ultrasonic measurement system (pulser/receiver, cabling, transducers) so that it does not depend on the particular reference acoustic/elastic transfer function used to determine it. Schmerr *et al.* have demonstrated this fact for a number of different reference setups [10]. This means that the same system function can be used in conjunction with different acoustic/elastic transfer functions to determine the output voltage as long as the system settings (gain, *etc.*) are not changed and the same components (transducers, cabling, *etc.*) are present. For example, the system function found with the pitch-catch setup of Fig. 2(b) could also be used in Eq. (1.5) or Eq. (1.7) for the flaw measurement setup of Fig. 1.

It is also possible to determine the system function by characterizing all the elements that it contains. For example, the pulser part of the pulser/receiver can be modeled as a Thévenin equivalent voltage source, $V_i(f)$, and electrical impedance, $Z_i^e(f)$ as shown in Fig. 3(a) [3]. Similarly the receiver can be modeled as an electrical impedance, $Z_0^e(f)$, and a gain factor, $K(f)$, as shown in Fig. 3(b), where $K(f) = V_R(f)/V_0(f)$ [3]. All of these parameters can be determined experimentally through a series of voltage and current measurements so that both the pulser and receiver can be modeled explicitly in this fashion, assuming they act as linear devices.

The cabling used for both sound generation and reception can be modeled as linear two port systems as shown in Figs. 4(a), (b) [3]. On the sound generation side the voltage and current $(V_p(f), I_p(f))$ at the output port of the pulser can be related to the voltage and current $(V_{in}(f), I_{in}(f))$ at the electrical input port of the transmitting transducer through a 2x2 transfer matrix, $[\mathbf{T}]$, *i.e.*

$$\begin{Bmatrix} V_p \\ I_p \end{Bmatrix} = \begin{bmatrix} T_{11} & T_{12} \\ T_{21} & T_{22} \end{bmatrix} \begin{Bmatrix} V_{in} \\ I_{in} \end{Bmatrix}. \quad (1.19)$$

On the reception side, the voltage and current $(V_t(f), I_t(f))$ at the electrical output port of the receiving transducer can be related to the voltage and current $(V_0(f), I_0(f))$ at the receiver input by another 2x2 transfer matrix, $[\mathbf{R}]$, *i.e.*

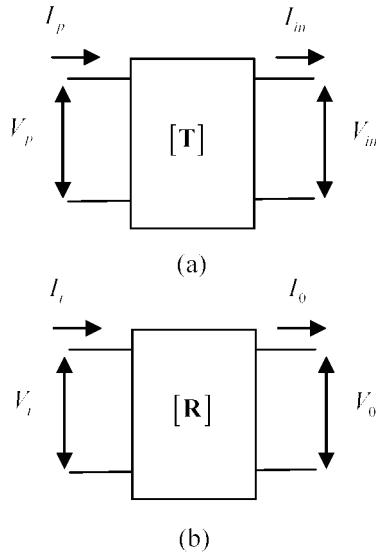


Figure 4. (a) A two port model of the cabling connecting the pulser and the transmitting transducer, and (b) a two port model of the cabling between the receiving transducer and the receiver.

$$\begin{Bmatrix} V_t \\ I_t \end{Bmatrix} = \begin{bmatrix} R_{11} & R_{12} \\ R_{21} & R_{22} \end{bmatrix} \begin{Bmatrix} V_o \\ I_o \end{Bmatrix}. \tag{1.20}$$

At the MHz frequencies found in NDE tests, unless the cables are very short (typically much less than a meter), the cables do not act as a pure pass-through devices, leaving the signals unchanged. Thus, typically the components of these transfer matrices are frequency dependent. Since a cable is a simple passive electrical device, these transfer matrix components can be easily obtained by making a series of voltage and current measurements of the cabling under different electrical termination conditions [4]. If we assume the cabling to act as linear, reciprocal devices we must have $\det[\mathbf{T}] = 1$, $\det[\mathbf{R}] = 1$ which are conditions on the transfer matrix components that can be used to check the measurements. Note that in some setups the cabling may consist of flexible cables and cabling contained in transducer support fixtures. All of these components can be characterized together *in situ*, using Eqs. (1.19) and (1.20) to model their transfer matrix.

Ultrasonic transducers are more difficult devices to characterize in an ultrasonic setup. In principle they could also be characterized as linear two port systems that transform electrical signals (voltage and current) into acoustic signals (force and velocity) and vice-versa. However, to date there has not been a

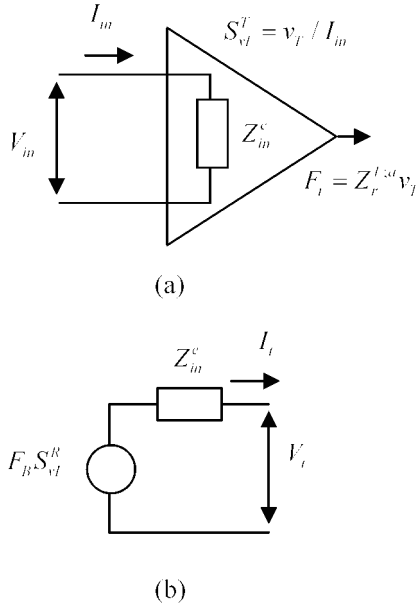


Figure 5. (a) A model of the transmitting transducer as an electrical impedance, $Z_{in}^{T:e}$, and a sensitivity, S_{vt}^T , and (b) the model of a receiving transducer and the acoustic sources that drive it as a voltage source, $F_B S_{vt}^R$, and an impedance, $Z_{in}^{R:e}$.

practical way to determine the components of the transducer transfer matrix in a fashion similar to what is done with the cabling. It is difficult, for example, to enforce different acoustic termination conditions at the transducer acoustic port and also to make the needed measurements of force and velocity. Fortunately, there is an alternate model one can use for the transmitting and receiving transducers that does not require knowledge of their transfer matrices, as shown in Figs. 5(a), (b). In Fig. 5(a) the transmitting transducer, T , is modeled as an electrical input impedance, $Z_{in}^{T:e}(f)$, and a sensitivity, $S_{vt}^T(f)$. The input impedance is just the ratio of the driving voltage and current at the transducer electrical input port, *i.e.* $Z_{in}^{T:e} = V_{in} / I_{in}$, and the sensitivity we will use here is defined as the ratio of the average output velocity, $v_T(f)$, at the acoustic output port of the transducer to the input current, *i.e.* $S_{vt}^R = v_T / I_{in}$. The output compressive force, $F_t(f)$, of the transducer is linearly related to the average output velocity through the acoustic radiation impedance of the transducer, $Z_r^{T:a}$, *i.e.* $F_t = Z_r^{T:a} v_T$. As discussed previously for piston transducers at high frequencies this acoustic radiation impedance is just the same value as that of a plane wave (although the transducer itself does not generate purely plane waves) so that if $v_T(f)$ is known the output force is also known. The reason why it is

useful to characterize the transducer in terms of its impedance and sensitivity is that both of these parameters can be obtained experimentally using purely electrical measurements. For example, consider a circular planar piston transducer in the pulse-echo configuration of Fig. 2(a). If one measures the frequency components of the voltage and current ($V_{in}(f), I_{in}(f)$) at the electrical input port of the transducer when it is radiating waves into the fluid but before any waves have been reflected from the fluid-solid interface, then from the definition of the transducer's impedance we have [13]

$$Z_{in}^{T:e}(f) = \frac{V_{in}(f)}{I_{in}(f)}. \quad (1.21)$$

In the same fashion, if one measures the frequency components of the voltage and current ($V_{out}(f), I_{out}(f)$) at the electrical output port of the transducer when it is receiving the beam of sound reflected from the fluid-solid interface, it can be shown that the sensitivity is given by [13]

$$S_{vt}^T(f) = \sqrt{\frac{V_{in}(f)I_{out}(f) + V_{out}(f)I_{in}(f)}{t_A(f)Z_r^{A:a}[I_{in}(f)]^2}}, \quad (1.22)$$

where $t_A(f)$ is the acoustic/elastic transfer function given by Eq. (1.8). Thus, with these two sets of electrical voltage and current measurements it is possible to obtain both the transducer's electrical impedance and its sensitivity. Knowledge of the transducer's electrical impedance defines its role as an electrical element in the generation of sound and knowledge of its sensitivity defines how the electrical inputs are transformed to acoustic outputs, so these two parameters (impedance, sensitivity) are all that is needed to fully characterize the role of the transducer as an electrical component and as a electrical-to-acoustic conversion device in the sound generation process.

When the ultrasonic transducer acts as a receiver, it converts the received acoustic waves into electrical signals. Remarkably, the same transducer impedance and sensitivity which we have defined for the case when the transducer is acting as a transmitter are also all that is needed to model the role of the transducer in the reception process. As illustrated in Fig. 5(b), it can be shown that a receiving transducer R and the acoustic waves that drive it can be modeled as a voltage source of strength $F_B S_{vt}^R$ in series with the electrical impedance, $Z_{in}^{R:e}$, where $F_B(f)$ is the *blocked force* acting on the receiving transducer by all the waves present [3]. By definition, this blocked force is just the compressive force exerted on the transducer face when that face is held rigid (motionless). This particular force appears naturally when modeling the sound

reception process and also appears in the definition of the acoustic/elastic transfer function as will be shown shortly.

Since we have shown that it is possible to characterize all the elements of both the sound generation and sound reception processes with simple models whose parameters can be obtained experimentally with a number of electrical measurements, one can combine all these models into explicit expressions for transfer functions that define the complete sound generation and reception processes. For example, if we define the sound generation transfer function, $t_G(f)$, as the ratio of the output compressive force, $F_t(f)$, on the face of the transmitting transducer to the Thévenin equivalent voltage source of the pulser, $V_i(f)$, it can be shown that [3] (see Fig. 6)

$$t_G(f) \equiv \frac{F_t(f)}{V_i(f)} = \frac{Z_r^{T:a} S_{vl}^T}{(Z_{in}^{T:e} T_{11} + T_{12}) + (Z_{in}^{T:e} T_{21} + T_{22}) Z_i^e}. \quad (1.23)$$

Similarly, if we define a sound reception transfer function, $t_R(f)$, as the ratio of the output voltage of the pulser, $V_R(f)$, to the blocked force, $F_B(f)$, we have (see Fig. 6) [3]

$$t_R(f) \equiv \frac{V_R(f)}{F_B(f)} = \frac{K Z_o^e S_{vl}^R}{(Z_{in}^{R:e} R_{11} + R_{12}) + (Z_{in}^{R:e} R_{21} + R_{22}) Z_o^e}. \quad (1.24)$$

The system function, $s(f)$, is then defined in terms of these transfer functions and the pulser source voltage as

$$\begin{aligned} s(f) &\equiv t_G(f) t_R(f) V_i(f) \\ &= \frac{Z_r^{T:a} S_{vl}^T}{(Z_{in}^{T:e} T_{11} + T_{12}) + (Z_{in}^{T:e} T_{21} + T_{22}) Z_i^e} \\ &\quad \cdot \frac{K Z_o^e S_{vl}^R}{(Z_{in}^{R:e} R_{11} + R_{12}) + (Z_{in}^{R:e} R_{21} + R_{22}) Z_o^e} V_i. \end{aligned} \quad (1.25)$$

By measuring all the elements contained in Eq. (1.25), it is possible to directly determine the system function. Of course, this result should agree with the direct measurement of the system function in a calibration setup, as discussed previously. Calculation of the system function in both of these ways has shown that they do indeed agree with each other [9, 14]. Equation (1.25) shows the very important role that the transducer sensitivity plays in the system function. In a pulse-echo setup where both the transmitting and receiving transducers are identical ($T = R$) the system function is proportional to the square of the

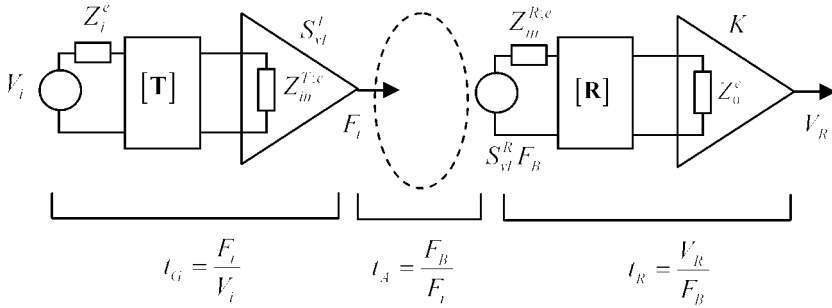


Figure 6. A complete model of an ultrasonic measurement system where the sound generation process can be described by a transfer function, t_G , the sound reception process by a transfer function, t_R , and all the acoustic/elastic propagation and scattering processes by the transfer function, t_A .

transducer sensitivity. Equation (1.25) also shows explicitly how the cabling properties and other electrical properties of the ultrasonic measurement system combine to generate the system function.

Having two methods to determine the system function gives us a set of very useful options. For example, in flaw measurement systems where we are primarily interested in the acoustic/elastic flaw signals, the direct determination of the system function by deconvolution (Eq. (1.18)) in conjunction with ultrasonic beam models and flaw scattering models gives us the ability to predict the measured flaw signals in an absolute manner. This approach allows us to efficiently study how the ultrasonic beam and flaw characteristics affect the measured response. In contrast, by synthesizing the system function directly from the measurement of its elements (Eq. (1.25)) one can study the effect that changes of system components and system settings have on the measured signals and optimize inspection setups, choice of transducers, *etc.* In the entire ultrasonic measurement system, the output voltage, $V_R(f)$, can be written as

$$\begin{aligned}
 V_R(f) &= \frac{V_R(f)}{F_B(f)} \frac{F_B(f)}{F_i(f)} \frac{F_i(f)}{V_i(f)} V_i(f) \\
 &= t_R(f) \frac{F_B(f)}{F_i(f)} t_G(f) V_i(f) \\
 &= s(f) \frac{F_B(f)}{F_i(f)},
 \end{aligned}
 \tag{1.26}$$

which, when comparing with Eq. (1.3), shows that the acoustic/elastic transfer function, $t_A(f)$, is given by

$$t_A(f) = \frac{F_B(f)}{F_t(f)}, \quad (1.27)$$

i.e. this transfer function is just the ratio of the blocked compressive force acting on the face of the receiving transducer to the compressive output force generated on the face of the transmitting transducer (Fig. 6). This is the definition used in obtaining all the acoustic/elastic transfer functions discussed previously. If we assume that the interactions of the incident waves on the receiving transducer with its receiving face can be treated as plane wave interactions, then the blocked force is given by [3]

$$F_B(f) = 2F_{inc}(f), \quad (1.28)$$

where $F_{inc}(f)$ is the compressive force acting on the receiving transducer generated by only the incident waves, *i.e.* $F_{inc}(f)$ is the compressive force acting on the area of the transducer if the transducer is absent. Since this plane wave interaction assumption is likely a good approximation in many cases, Eq. (1.28) provides a convenient wave to obtain the acoustic/elastic transfer function. For example, in calculating the acoustic/elastic transfer function for the pulse-echo reference setup of Fig. 2(a) the normalized average pressure, $p_{ave} / \rho_1 c_{p1} v_0$, generated at the transducer face by the sound beam reflected from the fluid/solid interface was modeled. This pressure can be used to determine the acoustic elastic transfer function since from Eq. (1.28) we have

$$t_A(f) = \frac{2p_{ave} S_T}{F_t} = \frac{2p_{ave} S_T}{Z_r^{T:a} v_0} = \frac{2p_{ave}}{\rho_1 c_{p1} v_0}, \quad (1.29)$$

where S_T is the area of the face of the transducer T and v_0 is the constant velocity acting on its face, assuming the transducer acts as a piston source. The factor of two appearing in Eq. (1.29) also appears in the diffraction correction term for this transfer function (see Eq. (1.9)) as well in the other acoustic/elastic transfer function expressions given previously for different reference setups because of Eq. (1.28) and the use of the blocked force in the definition of the acoustic/elastic transfer function.

Figure 6 gives a complete model of an ultrasonic measurement system. While Eq. (1.23) and Eq. (1.24) define explicitly the sound generation and reception transfer function in this complete model, calculation of the acoustic/elastic transfer function in a flaw measurement setup requires knowledge of both the propagating waves present in the measurement system and the waves scattered

from the flaw. In the next two sections we will discuss ultrasonic beam models and flaw scattering models that can give these wave fields.

4. Transducer Beam Models

In this section we will concentrate on the role that transducer beam models play in determining the acoustic/elastic transfer function. In the Thompson-Gray measurement model (Eq. (1.7)) acoustic/elastic beam models are needed to calculate the normalized velocity fields $\hat{V}_0^{(m)}(\mathbf{x}_0, f)$ ($m = 1, 2$) incident on a flaw in states (1) and (2) at a fixed point, \mathbf{x}_0 , that appear in that model. These same fields evaluated at an arbitrary point, \mathbf{x} , on the flaw surface, $\hat{V}^{(m)}(\mathbf{x}, f)$, are also implicitly present in the Auld form of the ultrasonic measurement model (Eq. (1.5)) since they are needed to determine the stress vectors and velocities present in that equation.

Modeling the velocity fields $\hat{V}^{(m)}(\mathbf{x}, f)$ is a difficult task since in many ultrasonic setups the sound beam generated by the transducer may interact with one or more interfaces and surfaces before it reaches a flaw. Here we will discuss beam models for the immersion setup shown in Figure 7 where the sound beam is generated by a planar piston transducer in a fluid and the sound must pass through a plane fluid-solid interface. This is a simple setup but one that will allow us to describe many of the main issues associated with beam modeling. In all the cases to be discussed we will treat the materials as perfect and neglect the attenuation of the ultrasound but attenuation can easily be introduced into the beam models as long as it is not too severe [1].

Most ultrasonic beam models express the transducer sound beam as a superposition of some simpler wave fields that act as set of fundamental basis functions. One choice of basis function is to express the waves generated by the transducer in the fluid by a superposition of plane waves and inhomogeneous waves traveling in different directions. This type of beam model is called an *angular plane wave spectrum beam model*. It is a convenient model to use when the fluid-solid interface is planar since it is possible to describe analytically how plane waves are transmitted or reflected at plane interfaces. For example, for the setup of Fig. 7 it can be shown that [1]

$$\hat{V}^{(m)}(\mathbf{x}, f) = \frac{f}{2\pi c_1} \iint_{S_T} \left[\int_{-\infty}^{+\infty} \int_{-\infty}^{+\infty} \frac{T_{12}(k_{1x}, k_{1y})}{k_{1z}} \cdot \exp \left[i(\mathbf{k}_2 \cdot (\mathbf{x} - \mathbf{x}_I) + \mathbf{k}_1 \cdot (\mathbf{x}_I - \mathbf{x}_T)) \right] dk_{1x} dk_{1y} \right] dS(\mathbf{x}_T), \quad (1.30)$$

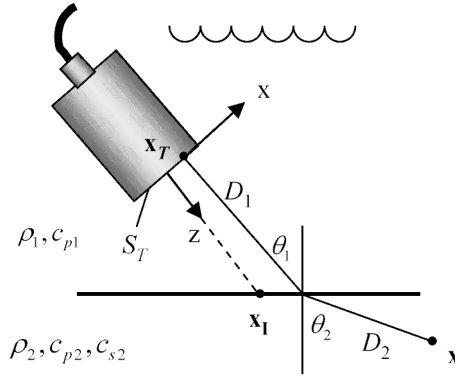


Figure 7. The radiation of a sound beam from a planar transducer through a plane fluid-solid interface.

where $(\mathbf{k}_1, \mathbf{k}_2)$ are the wave number vectors in the fluid and solid, respectively, T_{12} is the plane wave transmission coefficient for the fluid-solid interface (based on a velocity ratio). Point \mathbf{x} is an arbitrary point in the solid, point \mathbf{x}_T is an arbitrary point on the surface, S_T , of the transducer, and point \mathbf{x}_I is the point on the interface where a ray from the origin O along the central axis of the transducer face intersects the interface. The quantities (k_{1x}, k_{1y}, k_{1z}) are the components of the wave number vector in the fluid along the x -, y - and z -axes, respectively, (see Fig. 7 but note the y -axis is not shown explicitly in that figure) where k_{1z} is given by

$$k_{1z} = \begin{cases} \sqrt{k_1^2 - k_{1x}^2 - k_{1y}^2} & k_{1x}^2 + k_{1y}^2 < k_1^2 \\ i\sqrt{k_{1x}^2 + k_{1y}^2 - k_{p1}^2} & k_{1x}^2 + k_{1y}^2 \geq k_1^2 \end{cases} \quad (1.31)$$

[Note that strictly speaking we should identify the modes associated with quantities such as wave speeds and wave numbers in these wave field expressions since in the solid we can describe sound beams for both P-waves and S-waves. However, for economy of notation we will only designate these and other variables in this section by the material in which the waves are traveling. Thus, (c_1, c_2) will represent the wave speeds of waves traveling in media one and two, respectively, and (k_1, k_2) their corresponding wave numbers for whatever mode we are considering.] If the surface integral in Eq. (1.30) is defined as

$$C(k_{1x}, k_{1y}) = \iint_{S_T} \exp[-i\mathbf{k}_1 \cdot \mathbf{x}_T] dS(\mathbf{x}_T) \quad (1.32)$$

then for circular, elliptical, and rectangular transducers this integral can be done explicitly, leaving only the two infinite k -space integrals to be done

numerically [1]. In most cases the integrand values for only real values of k_{1z} are retained in Eq. (1.30) which corresponds to neglecting the inhomogeneous waves and reduces Eq. (1.30) to two finite integrals. Even with this assumption one must superimpose a large number of plane wave components so this beam model is numerically intensive.

An alternative approach is to make a high frequency approximation and evaluate the k -space integrals in Eq. (1.30) by the method of stationary phase. In this case, Eq. (1.30) reduces to a *Rayleigh-Sommerfeld* type of integral [1]

$$\hat{V}^{(m)}(\mathbf{x}, f) = \frac{if}{c_{p1}} \iint_{S_T} T_{12} \frac{\exp[ik_1 D_1 + ik_2 D_2]}{\sqrt{D_1 + \frac{c_2}{c_1} D_2} \sqrt{D_1 + \frac{c_2 \cos^2 \theta_1}{c_1 \cos^2 \theta_2} D_2}} dS, \quad (1.33)$$

where the distances (D_1, D_2) and angles (θ_1, θ_2) are calculated from a point \mathbf{x}_T on the face of the transducer to the point \mathbf{x} in the solid along a stationary phase (ray) path that satisfies Snell's law and the plane wave transmission coefficient, T_{12} , is evaluated for this same path (see Fig. 7). The ordinary Rayleigh-Sommerfeld integral for a single fluid medium is a superposition of spherical waves arising from point sources points distributed over the face of the transducer [1]. Similarly, Eq. (1.33) represents the wave field in the solid as a superposition of waves from point sources on the transducer face but the elastic waves in the solid in this case have elliptical wave fronts due to the interaction of the spherical waves in the fluid with the plane interface at oblique incidence. Because one must take many source points on the transducer surface to evaluate Eq. (1.33) accurately, like the angular plane wave spectrum beam model, this beam model is not very computationally efficient.

One way to develop a fast beam model is to introduce the paraxial approximation. Loosely speaking, this approximation assumes that the ultrasonic wave field can be described as a well-collimated beam where there is a single predominant propagation direction. In the first (fluid) medium this direction is normal to the face of the transducer. In the k -space integrations of Eq. (1.30) the paraxial approximation corresponds to assuming that $k_{1x}, k_{1y} \ll k_1$. If one introduces this paraxial approximation into Eq. (1.30) and one also uses Stokes' theorem to replace the surface integral over S_T by an explicit term and a line integral around the edge, C_T , of the transducer, one obtains a *boundary diffraction wave beam model* of the transducer wave field in the quasi-plane wave form [1]

$$\hat{V}^{(m)}(\mathbf{x}, f) = T_{12}^0 \exp(ik_1 D_{10} + ik_2 D_{20}) C(\mathbf{x}, f) \quad (1.34)$$

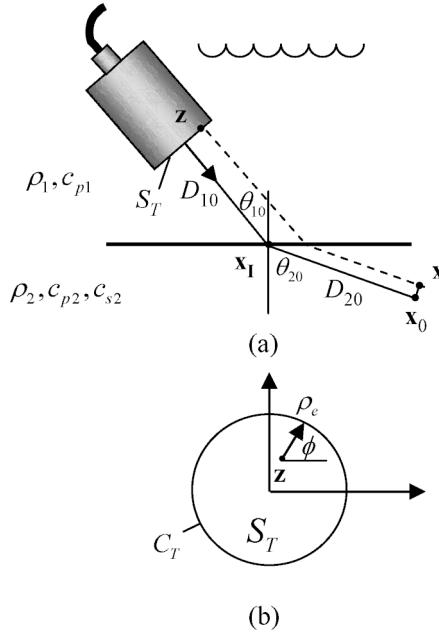


Figure 8. (a) Geometrical parameters that define the propagation of the waves from the transducer into the solid in the paraxial approximation, and (b) those parameters defined in the plane of the transducer.

where the diffraction correction, $\mathbb{C}(\mathbf{x}, f)$, is given by

$$\mathbb{C}(\mathbf{x}, f) = \frac{1}{\sqrt{\Delta_{x0}} \sqrt{\Delta_{y0}} C_T} \oint_{C_T} \left\{ \Theta(\mathbf{x}) - \exp \left[\frac{ik_1 \rho_e^2(\mathbf{x}, \phi)}{2} \left(\frac{\cos^2 \phi}{\Delta_{x0}} + \frac{\sin^2 \phi}{\Delta_{y0}} \right) \right] \right\} d\phi \quad (1.35)$$

$$\frac{\cos^2 \phi}{\Delta_{x0}} + \frac{\sin^2 \phi}{\Delta_{y0}}$$

and where

$$\Theta(\mathbf{x}) = \begin{cases} 1 & \mathbf{z} \text{ inside } S_T \\ 1/2 & \mathbf{z} \text{ on } C_T \\ 0 & \mathbf{z} \text{ outside } S_T \end{cases} \quad (1.36)$$

with

$$\Delta_{x0} = D_{10} + \frac{c_2}{c_1} D_{20} \quad (1.37)$$

$$\Delta_{y0} = D_{10} + \frac{c_2 \cos^2 \theta_{10}}{c_1 \cos^2 \theta_{20}}.$$

The distance $\rho_e(\mathbf{x}, \phi)$ is shown in Fig. 8(b). This distance is measured from a point, \mathbf{z} , on the plane of the face of the transducer to an arbitrary point on the edge of the transducer, where \mathbf{z} is the point obtained by tracing a ray (the dashed line in Fig. 8(a)) from \mathbf{x} to the plane of the transducer face along a ray that is parallel to the fixed ray that lies along the central axis of the transducer in the fluid and satisfies Snell's law (the solid line in Fig. 8(a)). The distances (D_{10}, D_{20}) and the plane wave transmission coefficient, T_{12}^0 , are calculated along the central axis ray. This boundary diffraction wave beam model is typically several orders of magnitude faster to compute than either the angular plane wave spectrum model or the Rayleigh-Sommerfeld model so that it can be used effectively as a beam model whenever plane interfaces are present. For curved interfaces, however, all of these beam models have difficulty in dealing with cases where focal points or caustics are present in the solid [1].

A beam model that is both fast and can handle curved interfaces is the multi-Gaussian beam model [15]. In this model, the basis functions used are Gaussian beams which have an advantage over plane waves or spherical waves in that they remain well-behaved even after transmission through curved surfaces and the laws that define their propagation and reflection /refraction can be obtained analytically. Also, by superimposing only ten Gaussian beams one can accurately represent the wave fields of circular piston transducers that are either planar or focused so there is very little computation required for a Gaussian beam model. Gaussian beam models do rely on the paraxial approximation so they can degrade if the conditions of that approximation are not satisfied (as with tightly focused probes, near critical and grazing angles, *etc.*).

For the interface problem of Fig 7 the transducer wave field of a circular planar piston transducer is given by the multi-Gaussian beam model in the same quasi-plane form of Eq. (1.34), where the diffraction correction is expressed as [15]

$$\mathbb{C}(\mathbf{x}, f) = \sum_{r=1}^{10} \frac{\sqrt{\det[\mathbf{M}_2(D_{20})]_r} \sqrt{\det[\mathbf{M}_1(D_{10})]_r}}{\sqrt{\det[\mathbf{M}_2(0)]_r} \sqrt{\det[\mathbf{M}_1(0)]_r}} \quad (1.38)$$

$$\cdot [V_1(0)]_r \exp \left[i \frac{k_1}{2} \mathbf{y}^T [c_1 \mathbf{M}_2(D_{20})]_r \mathbf{y} \right]$$

and the ten values of $[V_1(0)]_r$ and $[M_1(0)]_r$ ($r = 1, 2, \dots, 10$) can be related to a set of ten complex coefficients (A_r, B_r) given by

$$\begin{aligned}
 [V_1(0)]_r &= A_r \\
 [M_1(0)]_r &= \begin{bmatrix} \frac{iB_r}{c_1 \tilde{D}_R} & 0 \\ 0 & \frac{iB_r}{c_1 \tilde{D}_R} \end{bmatrix}
 \end{aligned} \tag{1.39}$$

where the Rayleigh distance $\tilde{D}_R = k_1 a^2 / 2$ in terms of the radius, a , of the transducer and $\mathbf{y} = \mathbf{x} - \mathbf{x}_0 = (y_1, y_2)$ is a vector in a plane perpendicular to the central ray of the transducer in the solid medium from point \mathbf{x}_0 on that central ray to point \mathbf{x} (see Fig. 8(a)). Wen and Breazeale [16] obtained the set of ten coefficients (A_r, B_r) appearing in Eq. (1.38). Those coefficients approximate the piston profile on the face of the transducer and generate through Eq. (1.38) a very accurate model of the transducer wave field except in the very near field. The propagation of the Gaussian beam in the fluid is given by the propagation law [15]

$$[M_1(D_{20})]_r = \begin{bmatrix} \frac{[\{M_1(0)\}_{11}]_r}{1 + D_{10}c_1 [\{M_1(0)\}_{11}]_r} & 0 \\ 0 & \frac{[\{M_1(0)\}_{22}]_r}{1 + D_{10}c_1 [\{M_1(0)\}_{22}]_r} \end{bmatrix}. \tag{1.40}$$

If the transducer is radiating through a curved interface where a principal axis of the surface is aligned with the plane of incidence of the transducer (the plane that contains the central transducer axis and the normal to the interface) the transmission law across the interface is [15]

$$[M_2(0)]_r = \begin{bmatrix} \frac{(\cos^2 \theta_1 + Kh_{11}) / \cos^2 \theta_2}{c_1 (D_{10} - i\tilde{D}_R / B_r)} & 0 \\ 0 & \frac{1 + Kh_{22}}{c_1 (D_{10} - i\tilde{D}_R / B_r)} \end{bmatrix}, \tag{1.41}$$

where

$$K = (D_{10} - i\tilde{D}_R / B_r) \left(\cos \theta_1 - \frac{c_1}{c_2} \cos \theta_2 \right) \quad (1.42)$$

and (h_{11}, h_{22}) are the principal curvatures in the plane of incidence and perpendicular to that plane, respectively.

Finally, the propagation law in the solid is [15]

$$[\mathbf{M}_2(D_{20})]_r = \begin{bmatrix} \frac{[\{\mathbf{M}_2(0)\}_{11}]_r}{1 + D_{20}c_2 [\{\mathbf{M}_2(0)\}_{11}]_r} & 0 \\ 0 & \frac{[\{\mathbf{M}_2(0)\}_{22}]_r}{1 + D_{20}c_2 [\{\mathbf{M}_2(0)\}_{22}]_r} \end{bmatrix}. \quad (1.43)$$

Thus, with the (A_r, B_r) coefficients and these propagation/transmission laws, all the terms in Eq. (1.38) are explicitly known.

In exactly the same fashion a multi-Gaussian beam model can be constructed for generally oriented curved interfaces and multiple solid media, including anisotropic elastic solids. Rectangular transducers and spherically focused and cylindrically focused transducers can also be easily simulated with a multi-Gaussian beam model. Thus, a multi-Gaussian beam model is often the beam model of choice to simulate ultrasonic transducer wave fields.

The plane waves, spherical waves, and Gaussian beams discussed above are the basis functions most commonly used to generate ultrasonic beam models. Other more direct numerical methods such as finite elements [17], boundary elements [18], finite differences [19], and the finite elastodynamic integration (EFIT) technique [20] can also be applied but in general those methods are computationally intensive which severely limits their use in conducting significant parametric studies.

5. Flaw Scattering Models

In the general ultrasonic model of Eq. (1.5), if we assume that the incident waves in states (1) and (2) can be described by the quasi-plane wave forms of Eq. (1.6) but if we do not assume that the variations of these incident waves over the surface of the flaw are negligible, that measurement model becomes

$$V_R(f) = s(f) \left[\frac{4\pi\rho_2 c_{\alpha 2}}{-ik_{\alpha 2} Z_r^{T;a}} \right] \int_{S_f} \hat{V}^{(1)}(\mathbf{x}, f) \hat{V}^{(2)}(\mathbf{x}, f) \mathcal{A}(\mathbf{x}, f) \exp[ik_{\alpha 2} \mathbf{e}^{(2)} \cdot \mathbf{x}] dS(\mathbf{x}) \tag{1.44}$$

with

$$\mathcal{A}(\mathbf{x}, f) = \frac{1}{4\pi\rho_2 c_{\alpha 2}^2} \left[\tilde{\tau}_{ji}^{(1)} d_i^{(2)} + C_{ijkl} d_k^{(2)} (e_l^{(2)} / c_{\alpha 2}) \tilde{v}_i^{(1)} \right] n_j, \tag{1.45}$$

where C_{ijkl} is the elastic constant tensor for the material surrounding the flaw and n_j are the components of the outward unit normal on the flaw surface. The quantities $(\tau_{ij}^{(1)}, v_i^{(1)})$ are the stresses and velocity components on the surface of the flaw due to both the incident and scattered waves and the normalized quantities $(\tilde{\tau}_{ij}^{(1)}, \tilde{v}_i^{(1)})$ appearing in Eq. (1.45) are defined as

$$\begin{aligned} \tilde{\tau}_{ij}^{(1)} &= \frac{-2\pi i f \tau_{ij}^{(1)}}{v_r^{(1)} \hat{V}^{(1)}} \\ \tilde{v}_j^{(1)} &= \frac{-2\pi i f v_j^{(1)}}{v_r^{(1)} \hat{V}^{(1)}}. \end{aligned} \tag{1.46}$$

Physically, these normalized fields are the stresses and velocity components due to an incident quasi-plane wave of unit amplitude incident on the flaw.

Writing the measurement model in this manner is revealing as, like the Thompson-Gray measurement model, we see the ultrasonic beam model terms appear explicitly in Eq. (1.44). The quantity $\mathcal{A}(\mathbf{x}, f)$ thus contains the flaw scattering response. However, unlike the Thompson-Gray measurement model we see that the beam model terms and flaw scattering response cannot be treated separately in Eq. (1.44) as they must be integrated together over the flaw surface. Comparing Eq. (1.7) and Eq. (1.44) we see that the far-field scattering amplitude component, $A(f)$, appearing in the Thompson-Gray measurement model is given by

$$A(f) = \int_S \mathcal{A}(\mathbf{x}, f) \exp(ik_{\alpha 2} \mathbf{e}^{(2)} \cdot \mathbf{x}) dS(\mathbf{x}). \tag{1.47}$$

In an elastic solid, the incident waves that strike a flaw can be either P- or S-waves. In the far-field of the flaw the scattered waves are both spherical P- and S-waves. For an incident plane wave of type β ($\beta = p, s$) and scattered waves of type α ($\alpha = p, s$) the scattered displacement vector, \mathbf{u} , in the far-field is given by [1]

$$u(\mathbf{x}, f) = \mathbf{A}^{p;\beta} U_0 \frac{\exp(ik_{p2}r)}{r} + \mathbf{A}^{s;\beta} U_0 \frac{\exp(ik_{s2}r)}{r}, \quad (1.48)$$

where U_0 is the displacement amplitude of the incident wave, (k_{p2}, k_{s2}) are the wave numbers for scattered P-waves and S-waves, respectively, and r is the radial distance from a fixed point on the flaw, usually taken as the flaw “center” to point \mathbf{x} . The quantities $\mathbf{A}^{\alpha;\beta}$ are the *far-field vector scattering amplitudes* of the flaw. These vector scattering amplitudes can be expressed as integrals of the stress and velocity fields over the surface of the flaw from which it is easy to show that for a given set of incident and scattered waves (i.e. for specified α and β wave types) we have [1]

$$A(f) = \int_S \mathcal{A}(\mathbf{x}, f) \exp(ik_{\alpha 2} \mathbf{e}^{(2)} \cdot \mathbf{x}) dS(\mathbf{x}) = \mathbf{A}^{\alpha;\beta} \cdot (-\mathbf{d}^{(2)}), \quad (1.49)$$

where recall $\mathbf{d}^{(2)}$ is the polarization of the wave incident on the flaw from the receiving transducer (acting as a transmitter) in state (2). It is only in the Thompson-Gray model that this specific component of the vector scattering amplitude appears explicitly, but even in the more general case, as Eq. (1.49) shows, the quantity $\mathcal{A}(\mathbf{x}, f)$ is also closely related to this same component.

Obtaining either $\mathcal{A}(\mathbf{x}, f)$ or $A(f)$ is a challenging task since real flaw morphologies are often not simple and to find the stresses and velocities on the flaw surface rigorously it is necessary in general to solve a complex boundary value problem. Numerical methods such as boundary elements or finite elements may often be required to obtain these wave fields but one can obtain some useful flaw scattering with approximations. Here we will describe some results that have been obtained with the *Kirchhoff approximation*.

The Kirchhoff approximation assumes that on that part of the flaw surface, called the lit surface, S_{lit} , where the incident wave (assumed to be planar) can strike the surface directly, the scattered fields are given by the reflected and transmitted plane waves calculated at a plane interface whose normal locally coincides locally with the normal to the surface of the flaw at every point on the lit surface. On the remaining part of the flaw surface it is assumed that the total fields are identically zero. Since the interactions of a plane wave with a plane interface is a problem that can be solved analytically, using the Kirchhoff approximation leads to an explicit expression for $\mathcal{A}(\mathbf{x}, f)$ and hence an integral expression for $A(f)$ [1]. Recently it has been shown that for the pulse-echo response of an arbitrary stress-free flaw in an elastic solid, where the scattered wave direction is directly opposite to the incident wave direction, $\mathbf{e}^{(1)}$, in state (1),

the Kirchhoff approximation for $A(\mathbf{x}, f)$ is identical to the same pulse-echo response for a void in a fluid [21], namely

$$A(\mathbf{x}, f) = \frac{-ik_{\beta 2}}{2\pi} (\mathbf{e}^{(1)} \cdot \mathbf{n}) \exp \left[ik_{\beta 2} (\mathbf{e}^{(1)} \cdot \mathbf{x}) \right], \quad (1.50)$$

where in pulse-echo we have set the incident wave and scattered wave modes equal ($\alpha = \beta$) and $k_{\beta 2}$ ($\beta = p, s$) are the wave numbers for the host material surrounding the flaw for P-waves or S-waves, respectively. Thus, the pulse-echo scattering amplitude component, $A(f)$, for an arbitrary stress-free flaw in the Kirchhoff approximation is given for either P-waves or S-waves as

$$A(f) = \frac{-ik_{\beta 2}}{2\pi} \iint_{S_{in}} (\mathbf{e}^{(1)} \cdot \mathbf{n}) \exp \left[2ik_{\beta 2} (\mathbf{e}^{(1)} \cdot \mathbf{x}) \right] dS(\mathbf{x}). \quad (1.51)$$

There are a number of canonical stress-free geometries where Eq. (1.51) can be evaluated explicitly. For a spherical void (pore) of radius b we find [22]

$$A(f) = \frac{-b}{2} \exp(-ik_{\beta 2} b) \left[\exp(-ik_{\beta 2} b) - \frac{\sin(k_{\beta 2} b)}{k_{\beta 2} b} \right]. \quad (1.52)$$

For an elliptical flat crack with semi-major axes (b_1, b_2) along the unit vector directions $(\mathbf{u}_1, \mathbf{u}_2)$, respectively, [22]

$$A(f) = \frac{-ib_1 b_2 (\mathbf{e}^{(1)} \cdot \mathbf{n})}{2r_e} J_1(2k_{\beta 2} r_e), \quad (1.53)$$

where

$$r_e = \sqrt{b_1^2 (\mathbf{e}^{(1)} \cdot \mathbf{u}_1)^2 + b_2^2 (\mathbf{e}^{(1)} \cdot \mathbf{u}_2)^2}. \quad (1.54)$$

Finally, for a side-drilled hole of radius b and length L , which is a reference reflector commonly used in NDE, when the incident wave direction, $\mathbf{e}^{(1)}$, lies in a plane perpendicular to the axis of the hole we have [22]

$$A(f) = \frac{(k_{\beta 2} b)L}{2} \left[J_1(2k_{\beta 2} b) - iS_1(2k_{\beta 2} b) \right] + \frac{i(k_{\beta 2} b)L}{\pi}, \quad (1.55)$$

where S_1 is the Struve function. The beam variations over the length of a side-drilled hole in an ultrasonic measurement cannot normally be neglected, so that Eq. (1.55) cannot be used directly in the Thompson-Gray measurement model.

However, Schmerr and Sedov [23] have derived an equivalent measurement model that assumes that the beam variations are negligible only over the cross-section of the hole. In that case the general reciprocity-based measurement model reduces to

$$V_R(f) = s(f) \left[\int_L \hat{V}_0^{(1)}(z, f) \hat{V}_0^{(2)}(z, f) dz \right] \left[\frac{A(f)}{L} \right] \left[\begin{array}{c} 4\pi\rho_2 c_{\alpha 2} \\ -ik_{\alpha 2} Z_r^{T;a} \end{array} \right], \quad (1.56)$$

where $\hat{V}_0^{(m)}(z, f)$ are the normalized incident wave fields evaluated along the central z -axis of the side-drilled hole. For holes whose length exceeds the incident beam width the z -integrations in Eq. (1.56) are simply truncated at locations where the beam amplitude has become sufficiently small. Equation (1.55) can be placed into this measurement model to simulate the pulse-echo response of the side-drilled hole.

The Kirchhoff approximation can also be used to model the response of flaws with complex shapes. In those cases one must perform the integrations of the known fields over the lit surface numerically. However, if one evaluates the surface integral approximately at high frequencies with the method of stationary phase, an explicit expression can be derived for what is called the *leading edge response* of a volumetric (i.e. non crack-like) flaw. In a pulse-echo setup, for example, the leading edge response of a convex inclusion, A_{le} , for either P-waves or S-waves is given by [1]

$$A_{le}(f) = \frac{R_{12} \sqrt{R_1 R_2}}{2} \exp(-2ik_{\beta 2} d), \quad (1.57)$$

where R_{12} is the plane wave reflection coefficient at normal incidence to a planar interface between the host and flaw, (R_1, R_2) are the principal radii of curvature of the flaw surface at the stationary phase point, and d is the distance from a fixed point (usually taken as the “center” of the flaw) to where the constant phase plane of a propagating plane wave traveling in the incident wave direction first touches the flaw surface. Similar results can also be obtained for a more general pitch-catch setup. For very complex shaped non-convex flaws there may be multiple stationary phase points and hence multiple leading edge response contributions that must be obtained.

Since the magnitude of the leading edge response is a constant, this contribution to the total scattered wave response is present at all frequencies and is relatively insensitive to the limited bandwidth present in ultrasonic systems. In many cases, therefore, this leading edge response dominates the scattering response of even complex-shaped volumetric flaws.

We have given only a few examples of flaw scattering responses in this section, concentrating on cases where significant analytical results are possible with the Kirchhoff approximation. Other approximate methods such as the Born approximation [24], the geometrical theory of diffraction [25], and low-frequency approximations [26] also can yield useful results without resorting to brute force numerical methods.

6. Summary

As shown in this chapter we can model and/or measure all the elements of a typical bulk wave ultrasonic NDE system. The system function can be obtained by making a single output voltage measurement in a reference setup or by making a detailed set of electrical measurements of the electrical and electromechanical elements of the measurement system. The acoustic/elastic transfer function can be found with the use of ultrasonic beam models and flaw scattering models. Combining these models and measurements in a complete ultrasonic measurement model gives us the capability to make absolute predictions of the measured A-scan (voltage versus time) signals seen in ultrasonic flaw measurements. These developments make it practical to design, engineer, and optimize ultrasonic NDE systems at many levels. This model-based approach also provides the basis for making quantitative flaw evaluations, which in many cases is the end goal of ultrasonic NDE inspection efforts. Significant uses have already been made of this comprehensive ultrasonic measurement model and many more applications are possible in the future. By necessity, the discussion in this chapter has only outlined the main features of the underlying models and measurements. Much more detail can be found in [9].

References

1. L. W. Schmerr, *Fundamentals of Ultrasonic Nondestructive Evaluation – A Modeling Approach*, (Plenum, New York, N.Y., 1998).
2. J. S. Walker, *Fast Fourier Transforms, 2nd Ed.*, (CRC Press, New York, NY, 1996).
3. C. J. Dang, L. W. Schmerr and A. Sedov, *Research in Nondestructive Evaluation*, **14**, 141 (2002).
4. C. J. Dang, L. W. Schmerr and A. Sedov, *Research in Nondestructive Evaluation*, **14**, 177 (2002).
5. B. A. Auld, *Wave Motion*, **1**, 39 (1979).
6. D. O. Thompson and D. E. Chimenti, Eds., *Review of Progress in Quantitative Nondestructive Evaluation*, (Vols. 1-18, Plenum Press, N.Y. 1981-1999), (Vols. 19 – 24, (American Institute of Physics, Melville, N.Y., 2000-2006).
7. R. B. Thompson and T. A. Gray, *J. Acoust. Soc. Am.*, **74**, 140 (1983).
8. X. Chen and K. Q. Schwarz, *J. Acoust. Soc. Am.*, **95**, 3049 (1994).

9. L. W. Schmerr and S. J. Song, *Ultrasonic Nondestructive Measurement Systems – Models and Measurements*, (Springer, Cambridge, MA, 2007)
10. L. W. Schmerr, S. J. Song and H. Zhang, in *Nondestructive Characterization of Materials, VI*, Eds. R.E. Green Jr., K.J. Kozaczek and C. O. Ruud, (Plenum Press, New York, NY, 1994, p. 111.
11. H. J. Kim, J. S. Park, S. J. Song and L. W. Schmerr, *J. Nondestr. Eval.*, **23**, 81 (2004).
12. A. Papoulis, *Signal Analysis*, (McGraw-Hill, New York, NY., 1977).
13. A. Lopez-Sanchez and L. W. Schmerr, *IEEE Trans. Ultrasonics, Ferroelectrics and Frequency Control*, **53**, 2101 (2006)
14. A. L. Lopez-Sanchez and L. W. Schmerr, *Res. in Nondestructive Evaluation*, (2006, to appear).
15. R. J. Huang, L. W. Schmerr and A. Sedov, *Res. in Nondestructive Evaluation*, **16**, 143 (2005).
16. J. J. Wen and M. A. Breazeale, *J. Acoust. Soc. Am.*, **83**, 1752 (1988).
17. W. Lord, R. L. Ludwig and Z. You, *J. Nondestr. Eval.*, **9**, 155 (1990).
18. Q. C. Guo and J. D. Achenbach, *Ultrasonics*, **33**, 449 (1995).
19. H. Yim and E. Baek, “Two-dimensional numerical modeling and simulation of ultrasonic testing,” *J. Korean Soc. N.D.T.*, **22**, 649 (2002).
20. P. Fellingner, R. Marklein, K. J. Langenberg and S. Klaholz, *Wave Motion*, **21**, 47 (1995).
21. L. W. Schmerr and A. Sedov, in *Review of Progress in Quantitative Nondestructive Evaluation*, Eds. D.O. Thompson and D.E. Chimenti, (American Institute of Physics, Melville, NY, 22B, 2003) p. 1776.
22. A. Lopez-Sanchez, H. J. Kim, L. W. Schmerr and T. Gray, *Res. in Nondestructive Evaluation*, **17**, 49 (2006)
23. A. L. Lopez, H. J. Kim, L. W. Schmerr and A. Sedov, *J. Nondestr. Eval.*, **24**, 83 (2005).
24. J. E. Gubernatis, E. Domany, J. A. Krumhansl and M. Hubermann, *J. Appl. Phys.*, **48**, 2812 (1977).
25. J. D. Achenbach, A. K. Gautesen and H. McMaken, *Ray Methods for Waves in Elastic Solids*, (Pitman Books Ltd., Boston, 1982).
26. J. H. Rose, *Ultrasonics*, **25**, 141 (1987).